Journal Pre-proof

Enrichment of T-Lymphocytes from Leukemic Blood using Inertial Microfluidics towards Improved Chimeric Antigen Receptor-T Cell Manufacturing

Mona T. Elsemary , Michelle F. Maritz , Louise E. Smith , Majid Ebrahimi Warkiani , Benjamin Thierry

PII: S1465-3249(24)00714-X
DOI: https://doi.org/10.1016/j.jcyt.2024.05.005
Reference: JCYT 1775

To appear in: *Cytotherapy*

Received date: 29 February 2024
Accepted date: 5 May 2024

Please cite this article as: Mona T. Elsemary , Michelle F. Maritz , Louise E. Smith , Majid Ebrahimi Warkiani , Benjamin Thierry , Enrichment of T-Lymphocytes from Leukemic Blood using Inertial Microfluidics towards Improved Chimeric Antigen Receptor-T Cell Manufacturing, *Cytotherapy* (2024), doi: https://doi.org/10.1016/j.jcyt.2024.05.005

Enrichment of T-Lymphocytes from Leukemic Blood using Inertial Microfluidics towards Improved Chimeric Antigen Receptor-T Cell Manufacturing

Mona T. Elsemary[1], Michelle F. Maritz[1], Louise E. Smith[1], Majid Ebrahimi Warkiani[2], Benjamin Thierry[1*]

[1]*Future Industries Institute, University of South Australia Mawson Lakes Campus, Mawson Lakes, 5095, SA, Australia*

[2]*University of Technology Sydney, Broadway, Ultimo NSW 2007*

Correspondence: *Prof Benjamin Thierry, Future Industries Institute, Building X, University of South Australia, Mawson Lakes, Adelaide SA 5095, GPO Box 2471, Adelaide SA 5001, Australia*

benjamin.thierry@unisa.edu.au

Abstract

Chimeric antigen receptor (CAR-T) cell therapy is a successful immunotherapy for treatment of blood cancers. However, hurdles in their manufacturing remain including efficient isolation and purification of the T-cell starting material. Herein, we describe a one-step separation based on inertial spiral microfluidics for efficient enrichment of T-cells in B-cell acute lymphoblastic leukemia (ALL) and B-cell chronic lymphocytic leukemia (CLL) patient's samples. In healthy donors used to optimise the process, the lymphocyte purity was enriched from 65% (SD±0.2) to 91% (SD±0.06) and T-cell purity was enriched from 45% (SD±0.1) to 73% (SD±0.02). Leukemic samples had higher starting B-cell compared to the healthy donor samples. Efficient enrichment and recovery of lymphocytes and T-cells was achieved in ALL samples with B-cells, monocytes and leukemic blasts depleted by 80% (SD±0.09), 89% (SD±0.1) and 74% (SD±0.09) respectively, and a 70% (SD±0.1) T-cell recovery. CLL samples had lower T-cell numbers, and the separation process was less efficient compared to the ALL. This study demonstrates the use

of inertial microfluidics for T-cell enrichment and depletion of B-cell blasts in ALL, suggesting its potential to address a key bottleneck of the CAR-T manufacturing workflow.

Keywords: CAR-T, manufacturing, acute lymphoblastic leukemia, microfluidic, purification, phenotype

Introduction

Chimeric Antigen Receptor (CAR) T-cell therapy is one of the most compelling recent advances in cancer treatment. The clinical effectiveness of CAR-T cells has led to the U.S. Food and Drug Administration (FDA) approval of six drugs and their commercialization [1]. However, due to the inherent personalized nature and many complex steps involved in the preparation of CAR-T cells, large scale implementation of this cutting-edge immunotherapy remains challenging, and it is broadly accepted that further manufacturing advances are urgently required to realize its full potential [2–7].

Efficient enrichment of T-cells from peripheral blood is an essential initial step in CAR-T cell manufacturing. The percentage of T-cells after the initial separation step suffers from large patient-patient variation [8,9] which depends on many factors including the type of cancer , prior treatments, disease burden and method used for T-cell separation. In most cases, T-cell enrichment efficiency is much lower in cancer patients than in healthy individuals, as reported in several clinical trials [10,11] and by the oncologic advisory committee of the FDA [9].

This variability in the starting T-cell fraction significantly affects the time needed to produce the required CAR-T cell dose [12,13] and also makes it very difficult to standardize the manufacture process. The variability in leucocyte compositions within the starting cellular material was found

to have significant effects on the final T-cell product, encompassing aspects such as expansion, genetic modification, phenotypical composition, and clinical performance. For example, the presence of monocytes and red blood cells (RBCs) was shown to increase the percentage of CD4 T-cells, while high quantities of neutrophils decreased the percentage of CD4 T-cells [14]. The presence of granulocytes was shown to reduce the proliferation of T-cells and cytokine synthesis [15], while monocytes induce T-cell apoptosis [16] as well as interfere with magnetic bead binding and activation of T-cells [17]. Myeloid derived suppressor cells and natural killer cells were also shown to interfere with T-cell activation and expansion [18].

Most recently, the importance of depleting cancerous lymphocytes from healthy T-cells has been demonstrated, as these cells were shown to interfere with the transduction and expansion processes, and were associated to exhaustion of the CAR T-cell product [19–21]. The addition of B-cell receptor inhibitors during expansion was proposed to mitigate cancerous B-cells induced T-cell exhaustion [22]. Furthermore, a study highlighted that the transduction of contaminating leukemic B-cells could lead to treatment resistance [23]. This landmark study also reported that in leukemic patient's apheresis products, the percentage of leukemic B-cells varies significantly, and can reach up to 90%.

There is clearly a need for improved T-cell enrichment technologies able to yield high T cell purity while being compatible with cost-effective large-scale manufacturing. Current T-cell enrichment methods used in contemporary CAR-T cell manufacturing have their own advantages and limitations [24,25]. Ficoll separation based density fractionation of cellular populations is a well- established method that is still used occasionally in clinical trials [26]. It is however incapable of separating cells of similar densities as lymphocytes and monocytes [27]. A more clinically adopted separation method for T-cells is counterflow centrifugal elutriation, such as

the Rotea^{TM} and Terumo Elutra systems. Elutriation devices are used to produce several approved CAR T cells products, namely Kymriah, Yescarta, and Abecma. Elutriation separates lymphocytes from white blood cells in the leukapheresis product based on differences in cell size and density. Elutriation devices achieve acceptable recovery of the lymphocytes with high throughput [28] but have not been reported to separate T cells from cancerous B cells. Conversely, immunomagnetic T-cell separation is also commonly utilized for the manufacturing of CAR-T cells. For example, immunomagnetic enrichment of CD3+ T cells is used for Tecartus and Carvykti while separate enrichment of helper CD4+ T cells and cytotoxic CD8+ T cells is used in Breyanzi. Despite their ability to enrich specific T-cell subsets with high purity, immunomagnetic selection suffers from several drawbacks, including lack of robustness, high cost, limited throughput (less than 10^9 cells/hr) and variable recoveries depending on magnetic protocol used and donor disease state [10]. Additionally, the necessity to remove residual beads is a noted issue [29].

Towards addressing the limitations of conventional lymphocyte and T cells enrichment approaches, several microfluidic principles have been investigated, including electrokinetic methods [30], acoustophoresis [31–33] and magnetophoresis [34]. Microfluidics offer many advantages in the manufacturing of cellular product[35]. For example, microfluidic cell enrichment technologies can be readily fitted within sterile closed devices compliant with GMP standards and manufactured in the format of disposable cartridges [36]. Compared to large non-microfluidic cell sorters, they have lower void spaces and offer greater flexibility in processing volumes. This makes them very desirable in the pediatric leukapheresis applications where low extracorporeal volumes are processed [37]. Illustrating the potential of advanced microfluidic approaches, Curate Biosciences recently commercialized its microfluidic deterministic cell

separation system [38–40] and the Draper lab also signed an agreement with Kite Pharma to integrate their T-cell enrichment acoustic chips in the company cell therapy manufacturing platform [41,42]. Sony Biotech [43] have developed and commercialized a fluorescent activated cell sorting microfluidic chips for GMP compliant cell manufacture. Other companies developing closed GMP compliant systems include Aenitis technologies [44] and Cellular highways[45].

To address the critical bottleneck in the CAR-T cell manufacturing process, we evaluated the performance of inertial microfluidics in enriching T-cells and depleting other cells including leukemic blasts towards an efficient, cost-effective and high-throughput enrichment of T-cells in B-cell acute lymphoblastic leukemia (ALL) patients' blood samples. Our method relies on spiral inertial microfluidics, which is an established size and density based microfluidic cell sorter. Inertial microfluidic devices have been successfully implemented for the enrichment of circulating tumor cells from blood [46] and other cell types [47–50] and have been proven to be a high-throughput and versatile platform for cellular bioprocessing [51].

Materials and Methods

Device design, fabrication and operation

A low aspect ratio spiral microchannel device is comprised of two inlets and six outlets as illustrated in Figure 1. Two designs were tested, one with four turns (inner radius=0.8 cm, outer radius=1.2 cm) and one with eight turns (inner radius= 0.8 cm, outer radius= 2 cm). The polydimethylsiloxane (PDMS) spiral microchannel devices were fabricated using standard soft lithography from a SU-8 mold which was designed and fabricated by photolithography at the Australian National Fabrication Facility. Different microchannel heights were tested to modulate

the flow conditions ranging from 95 to 130 µm. Briefly, the devices were prepared by mixing the base and curing agent (Sylgard 184, Dow Corning Inc.) in a 10:1 ratio, pouring into the mold, degassing and then curing at 60ºC. The cured devices were released from the molds and input and output ports were punched using a 14-gauge puncher and then bonded to glass slides using air plasma (Harrick Plasma, USA). Two 15 cm inlet tubing were attached to the device and a syringe pump. Prior to cell separation, devices were treated with 1% bovine serum albumin (BSA) to minimize non-specific fouling [46]. Cells were mainly collected in outlets 2-6 whereas in outlet 1 only debris was collected and thus was not used in calculations thereafter. The recovery and purity of the different cell type (cell lines or a leukocyte fraction) in outlets 2-5 was calculated as follows:

Percentage Recovery of the Cell Type in outlets 2-5

$$= \frac{\text{Sum of the Cell Number of the Cell Type in Outlets } 2-5}{\text{Sum of the Cell Number of the Cell Type in all outlets}} \text{ X } 100$$

Percentage Purity of the Cell Type in outlets 2-5

$$= \frac{\text{Sum of the Cell Number of the Cell Type in Outlets } 2-5}{\text{Sum of Cell Number of all Cells in Outlets } 2-5} \text{ X } 100$$

Initial device optimization with cell lines

Cell lines were initially tested to assess the device operation and performance. Raji cells (CCL-86™, ATCC, USA) and A549 cells (CCL-185™, ATCC, USA) were cultured in complete RPMI medium (RPMI 1640 medium, 10% FBS, 1% glutamate, 1% penicillin/streptomycin) (Life technologies, Australia). Raji cells were sub-cultured and every two days, the cells were collected by centrifugation and then resuspended in fresh medium at 4 x 10^5 viable cells/mL. A549 cells were cultured in complete DMEM (DMEM medium, 10% FBS, 1% glutamate, 1% penicillin/streptomycin) (Life technologies, Australia) and subcultured at 70% confluence after

dissociating the cells with 0.025% trypsin and 0.01% EDTA (in PBS). All cells were cultured in T-75 culture flasks at 37ºC in a humidified atmosphere containing 5% (v/v) CO_2.

Device processing of leukocyte of healthy blood samples

Blood samples from healthy donors were collected in compliance with the University of South Australia Human Research Ethics Committee (protocol number: 201980) and then separated using Ficoll Paque Premium (GE Healthcare, USA) according to the manufacturer instructions to collect leukocytes. The blood was diluted with equal volume of Dulbecco Modified PBS and then layered carefully on top of the Ficoll Paque medium. The tubes were centrifuged at 400 × g for 40 min at 20°C. In order to simulate apheresis starting material (usually contains a mix of lymphocytes, monocytes and granulocytes) during optimization, both the mononuclear layer at the interface of the plasma (mainly lymphocytes and monocytes) as well as the granulocyte layer, located as a thin layer above the red blood cell (RBC) pellet, were collected and combined in the initial study. Cell suspensions were transferred to new tubes and washed with PBS + 1% FBS. Devices of different dimensions were tested but the eight turn device with a wall height of 100 and 130 μm was selected for the rest of this study. Ficoll paque was used for leukocyte separation to remove RBC and platelet contaminants which were not the main focus of this study.

Device separation of leukemic blood clinical samples

Cryopreserved B-cell chronic lymphocytic (CLL) and acute lymphoblastic leukemia (ALL) leukocyte samples were obtained from the South Australian Cancer Research Biobank (SACRB). These studies were approved by the University of South Australia Human Research Ethics Committee and the SACRB Specimen Access Committee (HREC 201777/ SACRB-APP-028). All patients provided informed consent in accordance with the Declaration of Helsinki.

Imaging Flow Cytometry

Cells were stained for immune cell surface markers, including the pan lymphocyte antiCD45 markers; FITC-antiCD45 (Raji cells) and leukocyte marker anti-human CD45 EF450 (clone HI30) (patient samples), T-cell marker; anti-human CD3 FITC (clone SK7), B-cell marker; anti-human CD19 APC (clone HIB19), monocyte marker anti-human CD14 PE (clone D3) (Life Technologies, Australia). Analyses were performed using either a BD Accuri flow cytometer or an ImageStreamx Mark II imaging flow cytometer (AMNIS, Seattle, WA, USA). Staining was performed in siliconized polypropylene tubes after resuspending cell pellets in ice cold PBS, 10% FBS and 1% sodium azide at a concentration of $2x10^7$ cells/mL. 0.1-10 µg/mL of the primary labelled antibodies were added and then incubated for 45 min at room temperature, after which the cells were washed and suspended in ice cold PBS, 10% FBS and 1% sodium azide and used for flow cytometry. Analysis of the cellular populations was performed using the IDEAS software Version 6.1 (AMNIS, Seattle, WA, USA) and FlowJo V10 (FLOWJO, USA). Cell size distributions was calculated using an adaptive erode mask (M04 CH04 77) on the AMNIS software, which allows a more accurate calculation of cell diameters (as shown in Figure 4c).

Cell Viability and Proliferation

Leukocyte viability was assessed before and after inertial microfluidic processing using Trypan Blue and PI exclusion staining, according to the manufacturer's instructions. Cell proliferation was determined by staining with the proliferation dye Carboxyfluorescein succinimidyl ester (CFSE) (Biolegend, Australia). Leukocytes were suspended at $2x10^6$ cells/mL in PBS and labeled with 10 µM CFSE for 10 min at 37°C. The reaction was stopped by adding an equal volume of FBS and incubation for 2 min at room temperature. The cells were then washed twice, and the CFSE-labeled cells were cultured for 48 hrs at 37°C and 5% CO_2 in 96-well microtiter

plates. To stimulate the proliferation of primary cells, especially the T-cells, the cells were activated using anti-CD3, anti-CD28 and IL-2 and the proliferation of the non-enriched leukocytes and the enriched leukocytes after separation was compared over 72 hrs at 24 hrs intervals. The proliferation index was then calculated using FlowJo software, which calculates it as the total number of divisions divided by the number of cells that went into division.

Statistical Analysis

All experiments were repeated at least three times and analysed non-parametrically using GraphPad Prism. The data was analysed using two-way ANOVA mixed model. For single variable experiments, the non-parametric Wilcoxon paired T-test was performed.

Results and Discussion

Optimization of size-based fractionation

Inertial microfluidics fractionates cells/particles based on how they experience different forces, depending on their physical characteristics, when flowing in spiral microfluidic devices, namely the net lift force (F_L) and the transverse Dean drag forces (F_D) [52]. The net lift force (F_L) increases with the diameter, while the counter Dean vortices, that are symmetric at the top and bottom of the microchannel, increase as the flow rate and channel height increases. The F_L/F_D experienced by cells/particles is proportional to the cube of the diameter (a_p^3). For larger cells/particles, the lift forces dominate, and they are focused near the inner wall. For lift forces to dominate, the ratio of the diameters to the channel height (a_p/H) is required to be larger than 0.07 [53,54]. The lower lift forces applied to smaller cells allow the Dean drag forces to dominate,

resulting in their enrichment away from the inner channel wall. The forces acting under different flow rate conditions are summarized in Figure 2

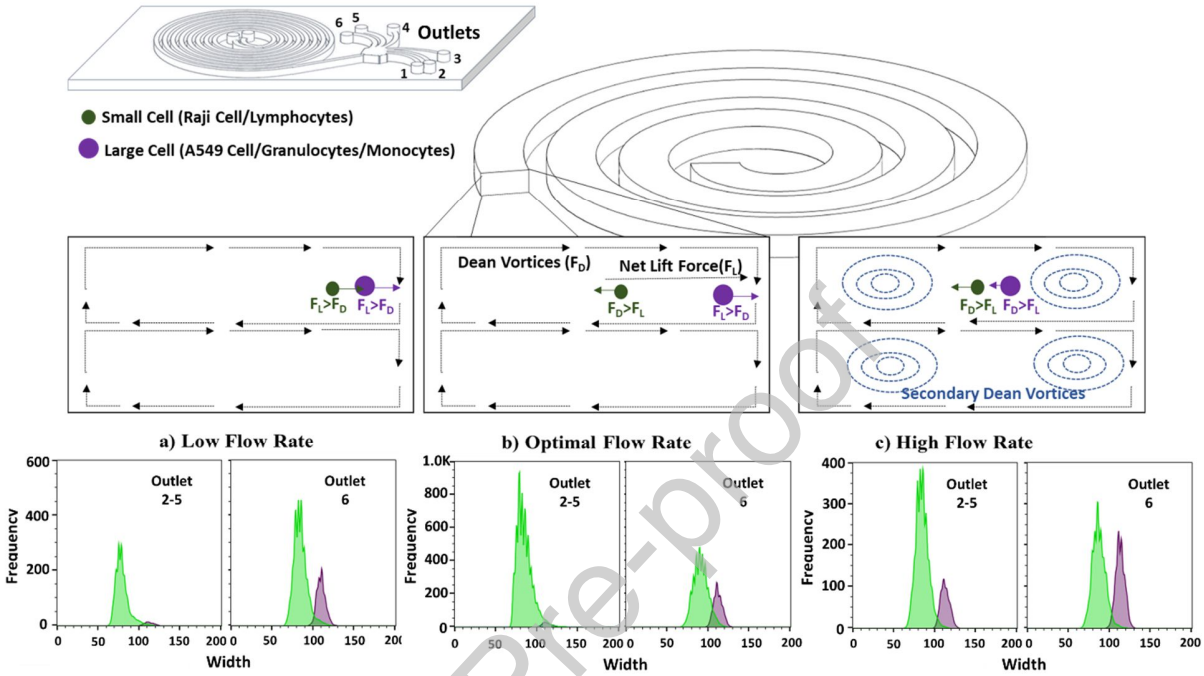

Figure 1. Schematic of forces acting on cells in inertial microfluidics. (a) At low flow rates, lift forces acting on both small and large sized cells are high, leading to inefficient separation and reduced recovery of small cells. (b) At optimum flow rates, lift forces acting on larger cells/particles only dominate, providing efficient separation. Larger cells were collected in the inner most channel (outlet 6), while smaller cells (e.g. lymphocytes) were enriched in outlets 2-5. (c) At high flow rates, strong dean vortices with Dean force predominating for both small and large cells/particles resulting in poor separation and reduced purity of small cells. Typical cell size histograms for Raji (green) and A549 (violet) model cells (The gating strategy used is shown in Supplementary Figure S1).

Towards optimizing the operation of the inertial microfluidic devices used in this study, we first evaluated the separation of a (2:1) mixture of two cell lines differing in size; Raji cells and A549 cells using an eight-turn inertial spiral microfluidic device (with a wall height of 130 μm). Raji cells, a B-lymphocyte derived cell line was used to mimic the smaller lymphocyte population in blood, while epithelial derived A549 cells were used to mimic the larger blood cells population, namely granulocytes and monocytes. Results following the testing of different flow rates ranging from 1.2 - 2.5 mL/min confirmed separation of larger and smaller size cells, with the larger A549 cells, typically collected as expected in the innermost channel (outlet 6), and the smaller Raji cells collected mainly in outlets 2-5 (Supplementary Figure S1 and Figure 1a-c). At flow rates between 1.8 and 2.2 mL/min, we achieved the highest purity and recovery of the smaller cell in outlets 2-5, with a recovery of 89% (SD±0.14) and purity of 82% (SD±0.16) at 2.2 mL/min (Supplementary Figure S1). At these optimal flow rates, the large sized cells experience mainly the lift forces, whereas smaller cells will be pushed by the dean drag forces away from the innermost wall, resulting in efficient separation, as illustrated in Figure 1b. Lower flow rates (1.2 to 1.8 mL/min) led to a decreased recovery of Raji cells in outlets 2-5, as more Raji cells shifted to outlet 6 (Figure 1a), due to the predominant lift forces acting on both small and large cells. At higher flow rates (2.5 to 2.8 mL/min), the effect was opposite, more A549 cells were collected with the Raji cells in outlets 2-5, resulting in lower purities, due to emergence of secondary dean vortices (Figure 1c). Building on this data, we next proceeded to systematically fine-tune the methodology using leukocytes collected from healthy donors.

Enrichment of lymphocytes from leukocytes in healthy donors

To fine-tune inertial microfluidic lymphocyte enrichment, leukocytes isolated from the blood of healthy donors were collected. First, the leukocyte composition and cell diameters were determined using imaging flow cytometry by staining with the pan lymphocyte antiCD45 marker, antiCD19- for B-cells, and antiCD3 for T-cells (Figure 2). Gating strategy for T- and B-cell populations is shown in Supplementary Figure S2. The mean diameter of T-cells was 7.3 µm (SD±0.06), 7.2 µm (SD±0.06) for B-cells and 8.6 µm (SD±0.25) for other white blood cells (monocytes and granulocytes and some other cells in the lymphocyte population).

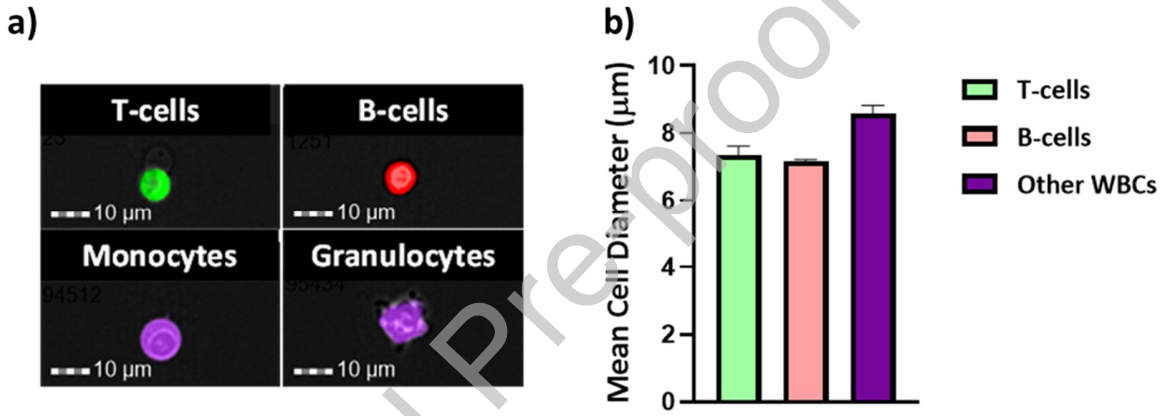

Figure 2. Leukocyte size distributions in healthy donors. Imaging flow cytometry: a) Composite images of T-cells (green, $CD45^{+ve}CD3^{+ve}CD19^{-ve}$), B-cells (red, $CD45^{+ve}CD3^{-ve}CD19^{+ve}$) and all other leukocytes (violet, $CD45^{+ve}CD3^{-ve}CD19^{-ve}$). b) Size distributions were calculated using an adaptive erode mask (M04 CH04 77) on the AMNIS software.

We next determined the optimal design and operating conditions to achieve the highest lymphocyte recovery and purity. To this end, leukocytes were resuspended in PBS+1%FBS and processed in inertial microfluidic devices under different conditions. High flow rates (1.8-2.2 mL/min) operation were not found to be optimal for Raji cell separation and therefore for smaller sized lymphocytes, hence we re-optimized the parameters focusing on lower flow rates. We first

tested the effect of different flow rates ranging from 1-1.5 mL/min in two device designs fabricated with heights of either 100 or 130 µm and calculated the purity and recovery of the lymphocytic fraction (outlet 2-5) (Figure 3, the lymphocytic fraction determined based on forward side scatter as explained in Supplementary Figure S3). At a flow rate of 1 mL/min, we achieved a higher purity (91% SD±0.06) using the 130 µm device compared to the 100 µm device (80% SD±0.05), although it was not statistically significant. However, the 100 µm device yielded a significantly lower recovery ranging from 16% - 57%, compared to a recovery ranging from 69% - 82% ($p<0.05$) for the 130 µm device at all three flow rates tested (Figure 3a and b). In the smaller channel height 100 µm device, the a_p/H ratio is higher than in the 130 µm device, causing higher lift forces to act on the smaller sized cells, leading to the shift of the smaller sized cells into the larger sized cell outlet and a reduction in purity.

As the 130 µm channel height device yielded more efficient separation than the 100 µm device, we performed further optimizations using the 130 µm device. The effect of the number of turns of the device was compared for different flow rates (Figure 3c). The longer 8-turn device resulted in a significantly higher purity, compared to the 4-turn device at all flow rates ($p<0.05$), with the highest purity of 91% SD±0.06 achieved for a flow rate of 1 mL/min. Efficient focusing of cells or particles of varying sizes in inertial microfluidics necessitates a specific downstream channel length. This length is dependent on both the size of the cells/particles and the hydraulic diameter, which, in turn, is influenced by the channel's width and height. [55]. Based on this data, the 8-turn device with a height of 130 µm was selected and used in the subsequent work.

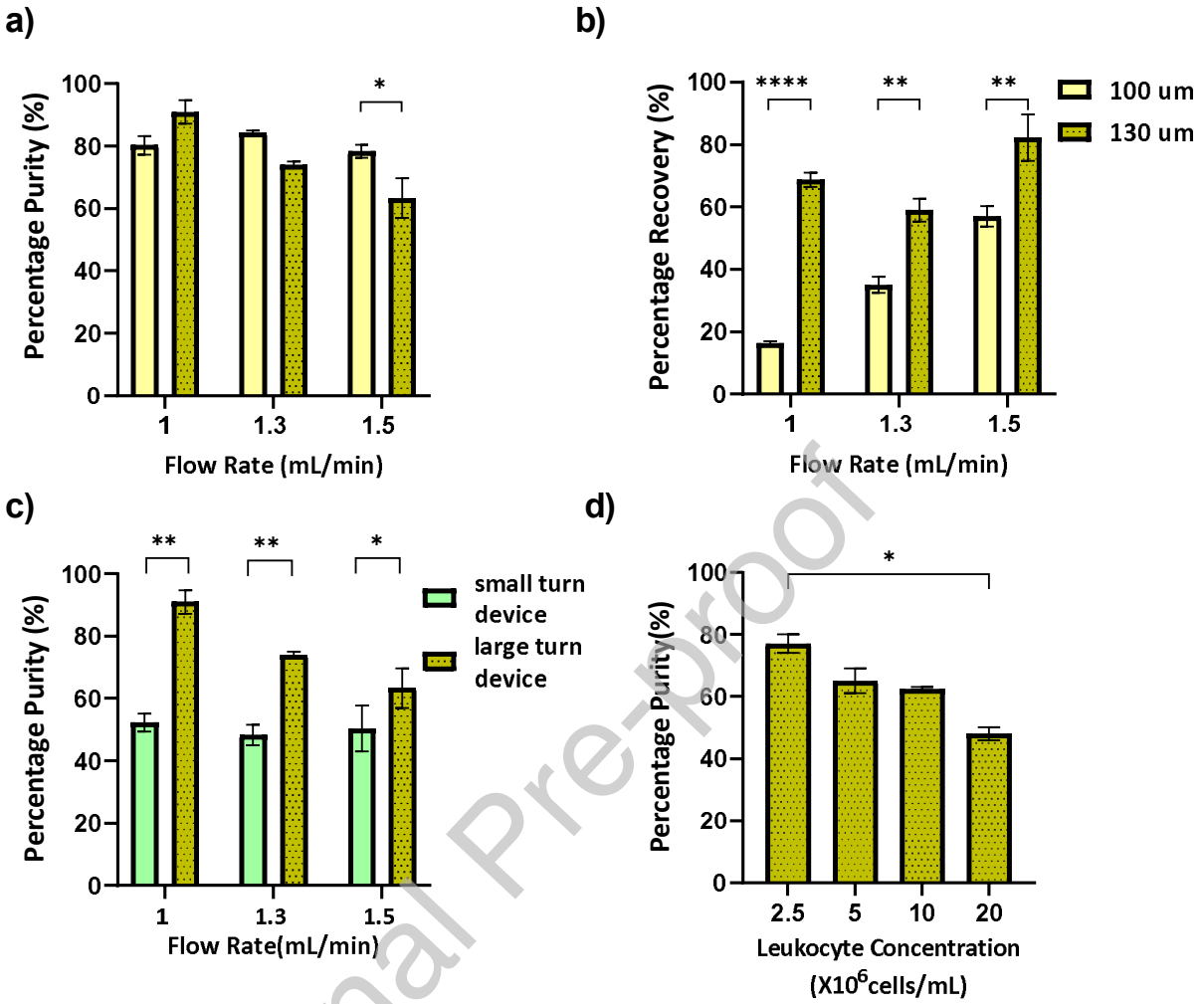

Figure 3. Optimization of the recovery and purity of lymphocytes from leukocytes isolated from healthy donors. Leukocytes in PBS+1%FBS were processed in the inertial microfluidic device and the percentage recoveries and purities for the lymphocytic enrichment outlets (outlets 2-5) is shown. Effect of flow rate in 100 and 130 µm channel height eight turn devices on a) purity and b) recovery. c) Effect of flow rates and devices' number of turns on purity (130 µm channel height). d) Effect of leukocyte concentration on purity in a 130 µm eight turn device (n=3, * $p<0.05$, ** $p<0.005$, **** $p<0.00005$).

The typical white blood cell concentrations in a typical apheresis product is $1x10^7$ to $1x10^8$ cells/mL [56]. To determine the cell concentration that can be operated in our inertial device, we tested cell concentrations ranging from $2.5x10^6$ to $20x10^6$ cells/mL (Figure 3d). As expected, the lower concentration of $2.5x10^6$ cells/mL resulted in the highest lymphocyte purity (77% SD±0.04), which was significantly greater compared to that obtained at the higher concentration of $20x10^7$ cells/mL (48% SD±0.03 $p<0.05$). The efficient separation of cells in inertial microfluidics relies on their neutral buoyancy. At higher concentrations, cell-cell interactions become more pronounced, causing disruptions in the focused streams of cells with varying sizes. As a result, the separation process becomes less effective. [55].

Under these optimal conditions (8-turn device with 130 µm channel height operated at a flow rate of 1 mL/min and with a feed leukocyte concentration of 2.5 to $5X10^6$ cells/mL), we achieved optimal recoveries and purities. From a starting lymphocyte purity of 65% (SD±0.2) and T-cell purity of 45% (SD±0.1), inertial microfluidic processing yielded a lymphocyte purity of 91 % (SD±0.06) and T-cell purity of 73% (SD±0.02) and recoveries of 63% (SD±0.04) and 60% (SD±0.22), respectively (Figure 4 b). While T-cells and B-cells were both collected in outlets 2-5, most of the other larger leukocytes (monocytes, granulocytes and large lymphocytes) were collected in outlet 6 (Figure 4b), yielding a depletion of 89% (SD±0.04). The mean cell diameter collected in outlets 2-5 was 7.2 µm (SD±0.2), compared to a mean diameter of 8.7 µm (SD±0.4) for cells collected in outlet 6. The extent of T-cell enrichment in outlet 2-5, as compared to outlet 6 before and after separation is shown in Figure 4b. These results confirmed that efficient inertial microfluidic lymphocyte enrichment can be achieved with a good recovery rate and depletion of larger leukocytes (monocytes and granulocytes) in healthy donor samples.

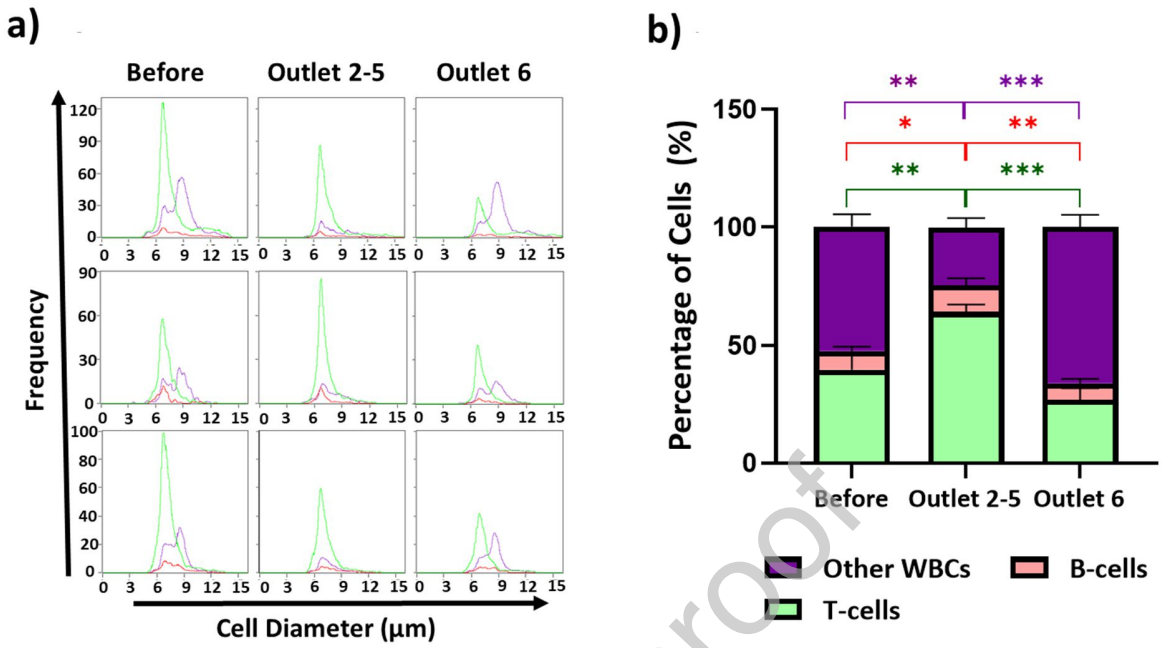

Figure 4. **Size distributions and enrichment of different leukocyte populations**. Leukocytes isolated from healthy donors were resuspended in PBS+1%FBS and processed in the inertial microfluidic device under optimized conditions a) Representative histograms of size distributions of the leukocyte subsets; T-cells (green), B-cells (red) and other WBCs (violet) before and after separation in the various device outlets as determined by imaging flow cytometry (shown for 3 independent donor batches). b) Cellular percentages before and after separation in the device showing enrichment of T-cells in outlets 2-5 and outlet 6 (n=7, * $p<0.05$, ** $p<0.005$, *** $p<0.0005$, Two-way ANOVA mixed model statistical analysis was used).

Inertial microfluidic T-cell enrichment in B-cell ALL and CLL patient samples

Leukemic samples are highly contaminated with cancerous cells and have highly variable ratios of the different white blood cell populations, which can be attributed to immunological responses to the disease [57]. To validate the efficiency of inertial microfluidics enrichment of T-cells from leukemic blood, we next assessed the utility and efficacy of our device using clinically relevant

samples from donor patients including B-lymphocyte ALL (n=6) and CLL (n=3) samples. Despite the target was to get hold of patient apheresis samples (having higher percentage of monocytes and granulocytes) however most of the collected leukemic samples were frozen vials of PBMCs (thence had a higher starting lymphocyte percentage 88% compared to the healthy donor ones in this study 65%).

As expected, the starting composition of the ALL and CLL samples varied between samples, but all had significantly larger numbers of B-cells over T-cells, in comparison to healthy donor samples (Figure 5). In healthy blood samples, B-cells comprise about 10% of the PBMC fraction [58]. In contrast, much higher percentages of B-cells (60% SD±0.3) and lower percentages of T-cells (30% SD±0.2) were found in the ALL samples (Figure 5b). Similarly, for the CLL samples, B-cells made up the majority 95% (SD±0.03) and only very low T-cell numbers were measured (5% SD±0.05), as shown in Figure 5c.

We next determined the T-cell and B-cell diameters in the ALL and CLL samples using imaging flow cytometry. The mean T-cell diameter in healthy blood samples (7.3 µm SD±0.3) was not statistically different to that of T-cells of the ALL (6.9 µm SD±0.7) and CLL (7.1 µm SD±0.3) samples. In contrast, the mean B-cell diameter of the ALL samples (8.3 µm SD±0.8) was significantly higher than that measured in healthy samples (7.2 µm SD±0.05, $p<0.05$). In contrast, B-cells from the 3 tested CLL samples only displayed minor size increase (7.5 µm SD±0.3). Importantly, the B-cell diameter (8.3 µm SD±0.8) in ALL samples was significantly larger than the T-cell diameter (6.9 µm SD±0.7, $p<0.05$), which provided the impetus for not only efficient inertial microfluidic enrichment of T cells but also depletion of cancerous B cells.

To confirm this hypothesis, the patients' samples were processed using the previously optimized conditions. For the ALL samples, the initial lymphocyte purity ranged from 70% to 99% with a

mean of 88% (SD±0.2) and the T-cell purity ranged from 7% to 53% with a mean of 36% (SD±0.2). After inertial microfluidic processing, we achieved a similar lymphocyte purity of 87% (SD±0.1) but significantly increased T-cell purity of 57% (SD±0.2) with a 70% (SD±0.1) T-cell recovery (Figure 6a). Remarkably, a 77% (SD±0.09) depletion of B-cells was determined. In four of these ALL samples, the T-cell purity increased by ~20% (from ~36% to ~ 57%), while in two of the patients the purity increased by ~40% (from ~24% to ~63%). These two patients also had a 90% depletion of B-cells. Variations in separation effectiveness among patients can be attributed to the distinct size distributions of T-cells and B-cells The majority of the B-cells in these two samples were large and therefore better differentiated from the T-cells, which allowed efficient separation. In the case of the remaining four samples, there was a range of overlap observed, as illustrated in Supplementary Figure S4. As noted above, the percentage of other white blood cells in the ALL samples was very low, however, in agreement with the data obtained with healthy blood samples, there was a significant depletion of monocytes (89% SD±0.1) and other white blood cells (60% SD±0.1).

Inertial microfluidic processing of the CLL samples was far less effective as shown in Figure 6b. In these samples, even though there was a good depletion of the non-lymphocytic white blood cell fraction (66%), only 55% of the B-cells were depleted. This is in agreement with the size measurements, as well the accumulation of small, non-apoptotic mature lymphocytes that have very low proliferation rate found in the blood of CLL patients [57,59–61]. In addition, the T-cells in the CLL samples are also slightly activated and adopt a dysregulated exhaustive phenotype [62], which may explain the relatively poor recovery of T-cells (47%). On the other hand, ALL is characterized by the presence of highly proliferating leukemic blasts that are significantly enlarged [63,64]. We therefore next endeavored to confirm that the significant enrichment of T-

cells in the ALL samples originates in the specific depletion of leukemic blasts during inertial microfluidic processing.

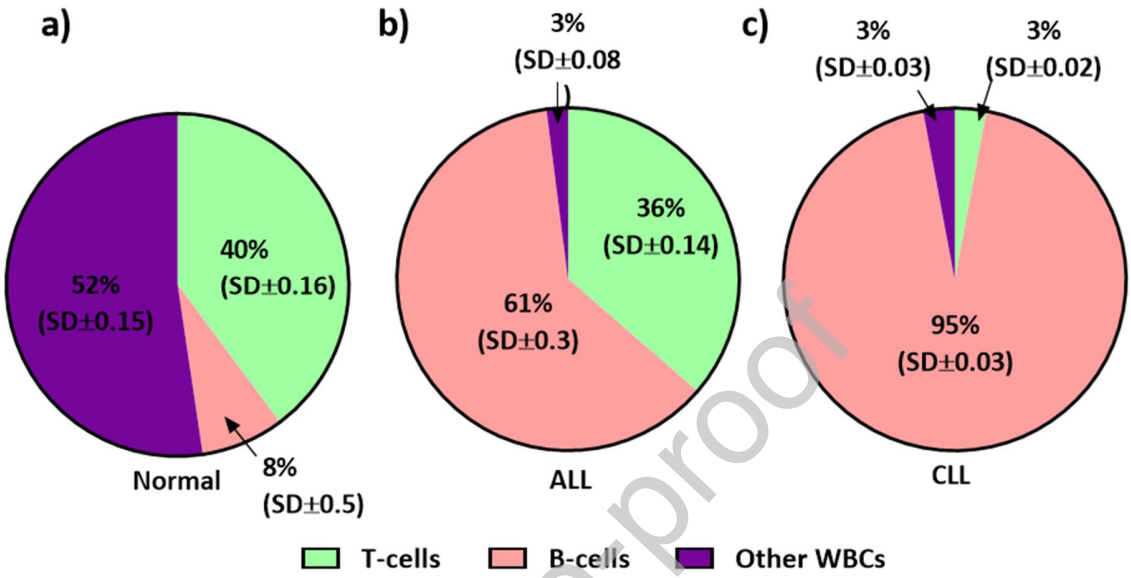

Figure 5. Pie charts comparing the percentage of leukocyte populations. Starting composition of isolated leukocytes used for isolation in the device a) Healthy donor sample (n=7) e; b) ALL donor samples (n=6); c) CLL donor samples (n=3).

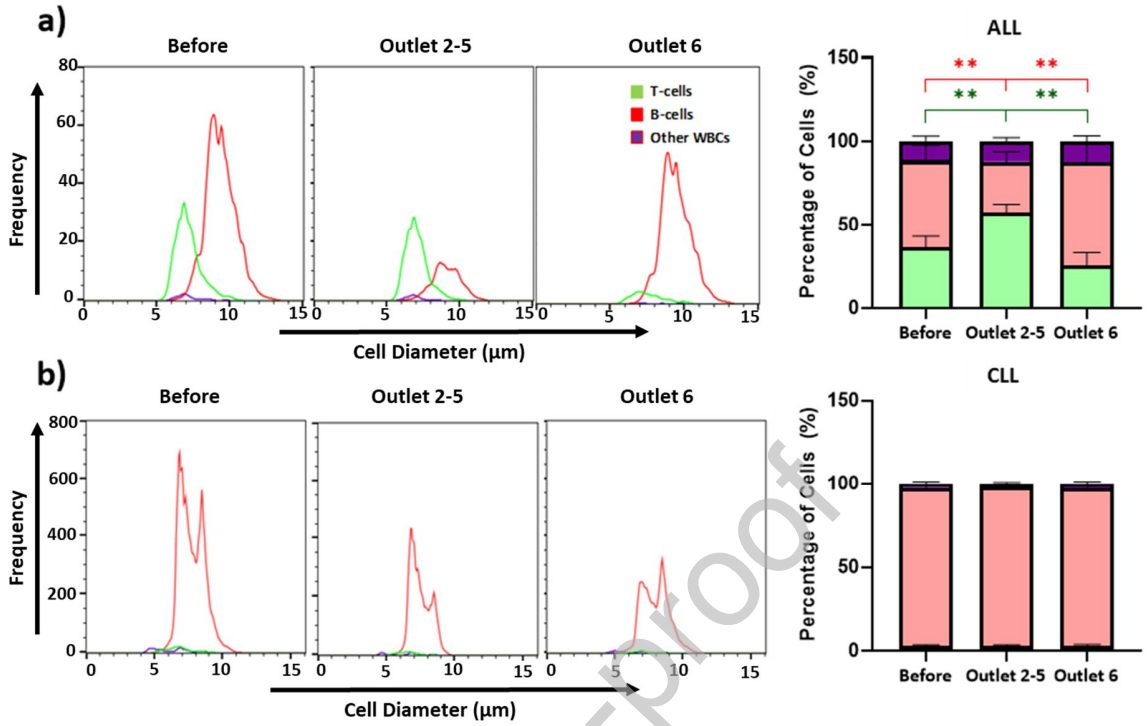

Figure 6. Relative enrichment of leucocyte populations in ALL and CLL donor samples. Leukemic PBMCs were resuspended in PBS+1%FBS and processed in the inertial microfluidic device under optimized conditions. Representative size distribution and cellular percentages showing the relative enrichment/depletion of leucocytes for a) ALL and b) CLL samples before and after separation in the various device outlets as determined by imaging flow cytometry. (n=6 for ALL and n=3 for CLL) Two-way ANOVA mixed model for paired data followed by Tukey multiple comparisons test was used, ** $p<0.005$,).

Depletion of leukemic blasts in ALL patient samples

Lymphoblasts were identified by CD45 dim/low side scatter characteristics according to Lacombe *et al.*,[65] which was confirmed by morphological analysis on the imaging flow cytometry. The number of leukemic blasts was investigated before and after inertial microfluidic processing. As shown in Figure 7, there was large variation in the initial frequency of cancerous

lymphoblasts of the total B-cell compartment (12%-88%) between patients' samples but in all cases, the number of blasts decreased significantly with an average depletion of 74% (SD±0.09, $p<0.005$) ranging from 56% -84% across the 6 ALL samples tested. The average B cell blast diameter was 8.8 µm (SD±0.5). It was also worth noting the presence of B-cells outside the blast gate, which were also large and efficiently depleted. Based on previous studies, these B-cells may also be blasts present outside of the blast gating [66,67,64] or highly proliferating non-malignant B-cells [68–70].

The substantial reduction in ALL lymphoblasts observed in this context holds significant potential importance, given their prevalence in leukemic apheresis products, along with other white blood cells [67,71]. The percentage of blasts differs according the type of leukemia, stage of disease, administration of prior treatments, as well as patients' age [72]. It is now well recognized that their presence negatively interferes with T-cell activation, transfection and expansion as well as result in T cell exhaustion[23,73–75]. To address this specific issue, Kite pharma recently developed a novel manufacturing process (XLP^{TM}) designed to enrich for T-cells, especially in malignancies with high burden of circulating B-lymphoblasts [76,77].

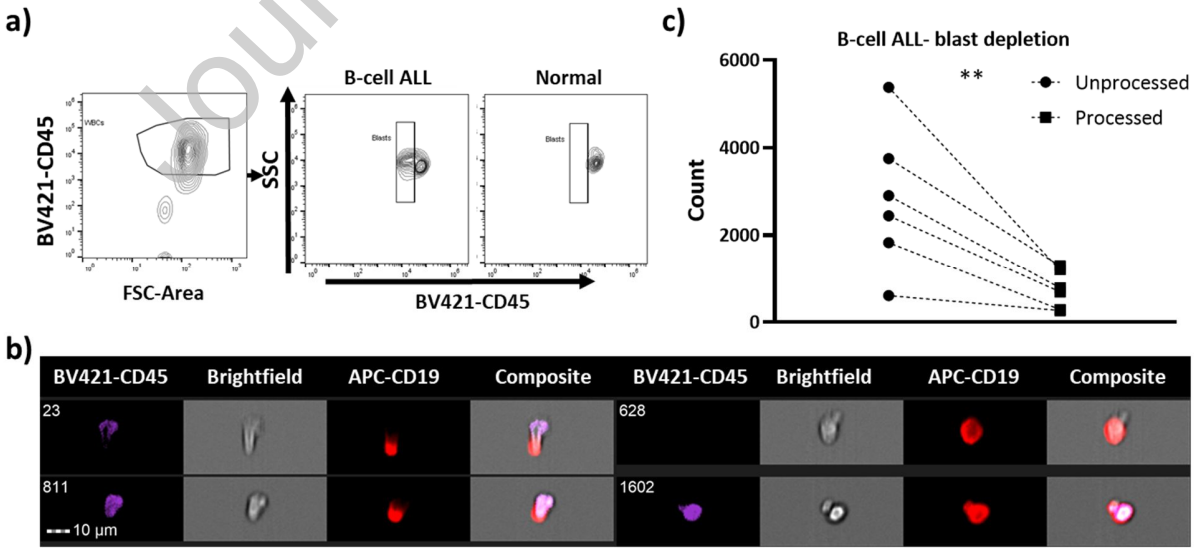

Figure 7. Depletion of leukemic blasts from B-cell ALL samples. a) Gating strategy for

identifying the leukemic blast population based on CD45 dim/low side scatter characteristics. b) Morphological confirmation of the leukemic blast population by imaging flow cytometry. c) Frequency of blasts before and after separation (Non-parametric Wilcoxon paired T-test analysis was performed; ** indicates statistically significant depletion at $p<0.005$, n=6).

Effect of inertial microfluidic processing on the viability and proliferation of T-cells.

To confirm that inertial microfluidic processing had no detrimental effects on T-cell viability and proliferation, we investigated the viability and proliferation of T-cells collected from outlets 2-5 at 0, 24 and 48 hr post device separation compared to the starting T-cell population (Figure 89). There was no difference in T-cell viability at all tested times (Figure 8a). Similarly, T-cell proliferation was also not affected (Figure 8b).

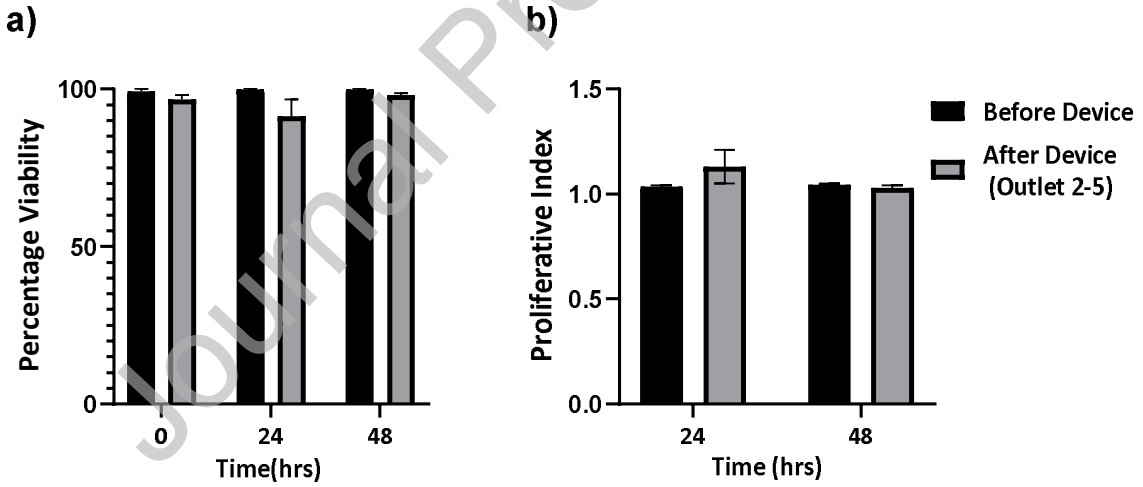

Figure 8. Effect of inertial microfluidic processing on T cells viability and proliferation. a) Cell viability, as measured by PI exclusion and b) Cell proliferation, as tested by CFSE staining of CD3 positive T-cells before and after device separation of outlet 2-5 (No statistically significant difference using paired t-test at $p<0.05$, n=3).

Effect of inertial microfluidic processing on T-cell phenotypes.

It is now well established that the phenotypes of CART-cell product influences to some extent clinical outcomes and that T-cells with less differentiated phenotypes are more preferable for manufacturing [78]. For example, naïve and central memory phenotypes displayed better *in vivo* persistence [79], while central memory phenotype were shown to have higher transfection efficiencies [80]. We therefore assessed the phenotypes of T-cells enriched from four ALL leukemic samples by staining for markers of helper CD4+ T-cells, cytotoxic CD8+ T-cells. We also stained for CD45RO and CCR7 to identify naïve ($CD45RO^{-}CCR7^{+}$), central memory ($CD45RO^{+}CCR7^{+}$), effector memory ($CD45RO^{+}CCR7^{-}$) and terminally differentiated effector cells ($CD45RO^{-}CCR7^{-}$ EMRAs). CD4+T-regulatory cells (T-regs) and CD8+T-suppressor cells (CD25+high, FOXP3+, CD127+ low) before and after inertial microfluidic processing were also assessed. Figure 9 provides a summary of the findings, highlighting notable variations among patients across different samples. While no statistically significant differences were measured in regards to the overall phenotypical compositions before and after processing, it is noteworthy that there was substantial depletion of CD4 T-regs in some of the samples, with an 87% depletion of T-regs in 2 of the 4 samples tested, while only 20% depletion was measured in the other two samples. It was also noted that CD8 T-suppressor cells were consistently depleted in all samples with an average 68% (SD±0.3) depletion. The substantial patient to patient variation in the depletion of T-reg and T-supp is likely due to differences in disease state and prior treatments for these patients, which affects the more activated and expanding cells in the immunosuppressive environment of the leukemic disease as reported by others [13,81–84]. ALL patients have a high concentration of T-regs in the blood due to the immunosuppressive nature of the cancer [85,86]. The presence of T-regs during ex vivo expansion can greatly affect the

proliferation of antigen active T-cells and the necessary development of effector T-cells, as shown in previous *ex-vivo* and *in-vivo* studies due to their immunosuppressive nature [87–90]. The potential of inertial microfluidic processing to deplete such phenotypes may be an added benefit and requires further investigation.

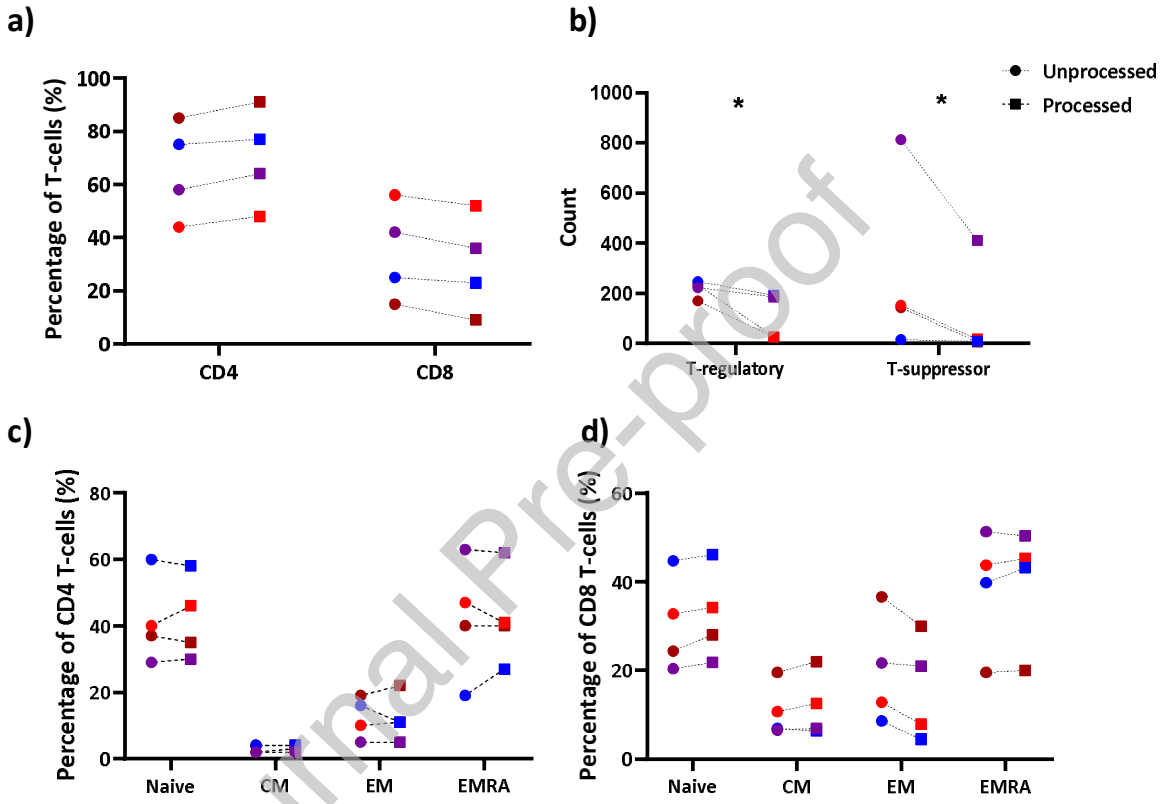

Figure 9. Effect of inertial microfluidic processing of B-cell ALL samples on the T-cell phenotypes. T-cell phenotypes before and after device separation of outlet 2-5 as determined by imaging flow cytometry. a) Percentage of CD4 and CD8; b) Number of CD4 T-regulatory and CD8 T-suppressor cells; c, d) Percentages of Naïve, central memory (CM), effector memory (EM) and terminally differentiated effector cells (EMRA) for c) CD4 and d) CD8. (Mixed model two-way ANOVA for paired data statistical analysis was used and no statistical significance was observed at $p<0.05$, $n=4$)

Translational potential in CAR-T cell manufacturing.

The optimized inertial microfluidic process developed in this study efficiently enriched T-cells and depleted B-cell blasts in ALL samples. The process also efficiently depleted larger sized white blood cellular contaminants as monocytes and granulocytes. Compared to other recently commercialized microfluidic platforms, the inertial microfluidic device was able to achieve a greater enhancement in T-cell purity compared to the Curate chip [40] while offering a greater recovery than that obtained with the Draper acoustophoretic chip [91] in addition to its ability in leukemic blast depletion. Importantly, the observed significant depletion of cancerous B cells is anticipated to perform well in other blood cancers where large B-cell blasts predominate, including acute myeloid leukemia [92], diffuse large B-cell lymphoma and other non-Hodgkin lymphomas [93]. We tested the effect of inertial microfluidic separation on the proliferation of the enriched T-cells and, in agreement with the relevant literature, we found no negative impact. We have also previously shown the feasibility of inertial microfluidic depletion of dead cells from a preclinical CAR-T cell product. Importantly, inertial microfluidic processing of CAR T cells did not affect their cytotoxicity and percentage of CAR positive T-cells [94]. While we have not attempted to prepare CAR T cells from the T cell fraction enriched from ALL patient samples, we anticipate no significant detrimental impact based on the available data and the brief and very mild conditions experienced by the cells during inertial microfluidic processing.

Inertial microfluidics is arguably a good compromise in regard to performance, cost and throughput between elutriation-based lymphocyte enrichment approaches and immunomagnetic bead selection. Microfluidic depletion of B-cell blasts offers a bead-less alternative to bead based depletion of B-cell contaminants, although further work is warranted to establish the relative

performance of inertial microfluidics against immunomagnetic selection. Microfluidic cell processing has the potential to facilitate decentralizing the manufacturing of cellular products, which could reduce cost by one seventh in the context of automation in a closed system with lower needs for personnel and clean room facilities[95–98]. While it is difficult to price a commercial device meeting the strict requirements associated to the manufacturing of a clinical grade cellular product, it is well established that single use disposable microfluidic devices can cost as little as 20 dollar per chip [99,100]. We therefore anticipate that in a scale-up commercial product would not add substantially to the overall cost of CAR T cell manufacturing compared to current technologies such as elutriation-based lymphocyte enrichment systems [99,100].

In order to appraise the translational potential of inertial microfluidics, one should consider the volumes of starting material being processed in typical CAR-T cell manufacture, which is usually in the order of 200- 600 mL [73,101]. Inertial microfluidic devices, despite their relatively limited processing volumes, offer a noteworthy advantage. By stacking multiple devices, it becomes possible to efficiently process large volumes. This approach has been successfully applied in the enrichment of circulating tumor cells, resulting in a remarkable 15-fold reduction in processing time. [102]. Using a similar approach would allow 15 mL/min processing, i.e. 200-600 mL of apheresis product would be processed within an acceptable time of 15-40 min. The concept of device stacking is commonly employed in cell separation to increase the throughput as had been presented by Curate Biosciences [39]and Draper [103].

Conclusion

An inertial microfluidic device could significantly increase the purity of T-cells from an average of 45% to 73% in white blood cell suspension mimicking apheresis like starting materials from

healthy donors. Despite the large variation in the cellular composition of the leukemia samples highly contaminated with B-cells, T-cells were effectively enriched from an average of 36% to 57% in ALL samples with over 80% depletion of leukemic B-cell blasts. Considering the relative simplicity of the process, the low cost of the underpinning microfluidic device and the anticipated relative ease of integration within closed GMP compliant system enabling automation, inertial microfluidics provide a compelling alternative to current T-cell enrichment methods used in the CAR T cell manufacturing process.

Acknowledgements

The authors acknowledge funding from the Australian Research Council Center of Excellence in Convergent Bio-Nano Science and Technology and the Cell Therapy Manufacturing Cooperative Research Center. This work was performed in part at the South Australian node of the Australian National Fabrication Facility under the National Collaborative Research Infrastructure Strategy to provide nano and microfabrication facilities for Australia's researchers.

Conflicts of Interest

The authors declare no conflict of interest.

References

[1] Chen Y-J, Abila B, Mostafa Kamel Y. CAR-T: What Is Next? Cancers (Basel) 2023;15:663. https://doi.org/10.3390/cancers15030663.

[2] Elsallab M, Maus MV. Expanding access to CAR T cell therapies through local manufacturing. Nat Biotechnol 2023;41:1698–708. https://doi.org/10.1038/s41587-023-01981-8.

[3] Blache U, Popp G, Dünkel A, Koehl U, Fricke S. Potential solutions for manufacture of CAR T cells in cancer immunotherapy. Nat Commun 2022;13:5225. https://doi.org/10.1038/s41467-022-32866-0.

[4] Ad F. The Challenge of Variability in Chimeric Antigen Receptor T cell Manufacturing. Regenerative Engineering and Translational Medicine 2020;6. https://doi.org/10.1007/s40883-019-00124-3.

[5] Egri N, Ortiz de Landazuri I, San Bartolomé C, Ortega JR, Español-Rego M, Juan M. CART manufacturing process and reasons for academy-pharma collaboration. Immunology Letters 2020;217:39–48. https://doi.org/10.1016/j.imlet.2019.10.014.

[6] Dai X, Mei Y, Nie J, Bai Z. Scaling up the Manufacturing Process of Adoptive T Cell Immunotherapy. Biotechnol J 2019;14:e1800239. https://doi.org/10.1002/biot.201800239.

[7] Iyer RK, Bowles PA, Kim H, Dulgar-Tulloch A. Industrializing Autologous Adoptive Immunotherapies: Manufacturing Advances and Challenges. Front Med 2018;5. https://doi.org/10.3389/fmed.2018.00150.

[8] Baguet C, Larghero J, Mebarki M. Early predictive factors of failure in autologous CAR T-cell manufacturing and/or efficacy in hematologic malignancies. Blood Advances 2024;8:337–42. https://doi.org/10.1182/bloodadvances.2023011992.

[9] Bryan WW. Tisagenlecleucel Novartis Pharmaceuticals Corporation 2017.

[10] Lock D, Mockel-Tenbrinck N, Drechsel K, Barth C, Mauer D, Schaser T, et al. Automated Manufacturing of Potent CD20-Directed Chimeric Antigen Receptor T Cells for Clinical Use. Hum Gene Ther 2017;28:914–25. https://doi.org/10.1089/hum.2017.111.

[11] Tumaini B, Lee DW, Lin T, Castiello L, Stroncek DF, Mackall C, et al. Simplified process for the production of anti-CD19-CAR engineered T cells. Cytotherapy 2013;15:1406–15. https://doi.org/10.1016/j.jcyt.2013.06.003.

[12] Teoh J, Brown LF. Developing lisocabtagene maraleucel chimeric antigen receptor T-cell manufacturing for improved process, product quality and consistency across CD19+ hematologic indications. Cytotherapy 2022:S1465-3249(22)00611-9. https://doi.org/10.1016/j.jcyt.2022.03.013.

[13] Li Y, Huo Y, Yu L, Wang J. Quality Control and Nonclinical Research on CAR-T Cell Products: General Principles and Key Issues. Engineering 2019;5:122–31. https://doi.org/10.1016/j.eng.2018.12.003.

[14] Elavia N, Panch SR, McManus A, Bikkani T, Szymanski J, Highfill SL, et al. Effects of starting cellular material composition on chimeric antigen receptor T-cell expansion and characteristics. Transfusion 2019;59:1755–64. https://doi.org/10.1111/trf.15287.

[15] Munder M, Schneider H, Luckner C, Giese T, Langhans C-D, Fuentes JM, et al. Suppression of T-cell functions by human granulocyte arginase. Blood 2006;108:1627–34. https://doi.org/10.1182/blood-2006-11-010389.

[16] Munn DH, Pressey J, Beall AC, Hudes R, Alderson MR. Selective activation-induced apoptosis of peripheral T cells imposed by macrophages. A potential mechanism of antigen-specific peripheral lymphocyte deletion. The Journal of Immunology 1996;156:523–32.

[17] Wang X, Borquez-Ojeda O, Stefanski J, Du F, Qu J, Chaudhari J, et al. Depletion of high-content CD14+ cells from apheresis products is critical for successful transduction and expansion of CAR T cells during large-scale cGMP manufacturing. Mol Ther Methods Clin Dev 2021;22:377–87. https://doi.org/10.1016/j.omtm.2021.06.014.

[18] Feng S, Cheng X, Zhang L, Lu X, Chaudhary S, Teng R, et al. Myeloid-derived suppressor cells inhibit T cell activation through nitrating LCK in mouse cancers. PNAS 2018;115:10094–9. https://doi.org/10.1073/pnas.1800695115.

[19] Cheng EL, Cardle II, Kacherovsky N, Bansia H, Wang T, Zhou Y, et al. Discovery of a Transferrin Receptor 1-Binding Aptamer and Its Application in Cancer Cell Depletion for Adoptive T-Cell Therapy Manufacturing. J Am Chem Soc 2022;144:13851–64. https://doi.org/10.1021/jacs.2c05349.

[20] Deng B, Pan J, Liu Z, Liu S, Chen Y, Qu X, et al. Peripheral leukemia burden at time of apheresis negatively affects the clinical efficacy of CART19 in refractory or relapsed B-ALL. Molecular Therapy - Methods & Clinical Development 2021;23:633–43. https://doi.org/10.1016/j.omtm.2021.10.006.

[21] Hoffmann J-M, Schubert M-L, Wang L, Hückelhoven A, Sellner L, Stock S, et al. Differences in Expansion Potential of Naive Chimeric Antigen Receptor T Cells from Healthy Donors and Untreated Chronic Lymphocytic Leukemia Patients. Front Immunol 2017;8:1956. https://doi.org/10.3389/fimmu.2017.01956.

[22] Stock S, Übelhart R, Schubert M-L, Fan F, He B, Hoffmann J-M, et al. Idelalisib for optimized CD19-specific chimeric antigen receptor T cells in chronic lymphocytic leukemia patients. Int J Cancer 2019;145:1312–24. https://doi.org/10.1002/ijc.32201.

[23] Ruella M, Xu J, Barrett DM, Fraietta JA, Reich TJ, Ambrose DE, et al. Induction of resistance to chimeric antigen receptor T cell therapy by transduction of a single leukemic B cell. Nature Medicine 2018;24:1499. https://doi.org/10.1038/s41591-018-0201-9.

[24] Stroncek DF, Lee DW, Ren J, Sabatino M, Highfill S, Khuu H, et al. Elutriated lymphocytes for manufacturing chimeric antigen receptor T cells. Journal of Translational Medicine 2017;15:59. https://doi.org/10.1186/s12967-017-1160-5.

[25] Wang X, Rivière I. Clinical manufacturing of CAR T cells: foundation of a promising therapy. Molecular Therapy - Oncolytics 2016;3:16015. https://doi.org/10.1038/mto.2016.15.

[26] Vormittag P, Gunn R, Ghorashian S, Veraitch FS. A guide to manufacturing CAR T cell therapies. Current Opinion in Biotechnology 2018;53:164–81. https://doi.org/10.1016/j.copbio.2018.01.025.

[27] Abou-el-Enein M, Elsallab M, Feldman SA, Fesnak AD, Heslop HE, Marks P, et al. Scalable Manufacturing of CAR T Cells for Cancer Immunotherapy. Blood Cancer Discovery 2021;2:408–22. https://doi.org/10.1158/2643-3230.BCD-21-0084.

[28] Stroncek DF, Lee DW, Ren J, Sabatino M, Highfill S, Khuu H, et al. Elutriated lymphocytes for manufacturing chimeric antigen receptor T cells. J Transl Med 2017;15. https://doi.org/10.1186/s12967-017-1160-5.

[29] Bateman CM, Antonenas V, Yehson K, Tong D, Hansra G, Clancy LE, et al. Results of Using Automated Clinimacs Prodigy for CD34 Selection from Mobilized Peripheral Blood Stem Cell Products. Blood 2017;130:3201–3201.

[30] Yang J, Huang Y, Wang X, Wang X-B, Becker FF, Gascoyne PRC. Dielectric Properties of Human Leukocyte Subpopulations Determined by Electrorotation as a Cell Separation Criterion. Biophysical Journal 1999;76:3307–14. https://doi.org/10.1016/S0006-3495(99)77483-7.

[31] Urbansky A, Olm F, Scheding S, Laurell T, Lenshof A. Label-free separation of leukocyte subpopulations using high throughput multiplex acoustophoresis. Lab Chip 2019;19:1406–16. https://doi.org/10.1039/C9LC00181F.

[32] Urbansky A, Lenshof A, Dykes J, Laurell T, Scheding S. Affinity-Bead-Mediated Enrichment of CD8+ Lymphocytes from Peripheral Blood Progenitor Cell Products Using Acoustophoresis. Micromachines (Basel) 2016;7:101. https://doi.org/10.3390/mi7060101.

[33] Lenshof A, Jamal A, Dykes J, Urbansky A, Astrand-Grundström I, Laurell T, et al. Efficient purification of CD4+ lymphocytes from peripheral blood progenitor cell products using affinity bead acoustophoresis. Cytometry A 2014;85:933–41. https://doi.org/10.1002/cyto.a.22507.

[34] Darabi J, Guo C. On-chip magnetophoretic isolation of CD4 + T cells from blood. Biomicrofluidics 2013;7. https://doi.org/10.1063/1.4821628.

[35] Kim H, Kim S, Lim H, Chung AJ. Expanding CAR-T cell immunotherapy horizons through microfluidics. Lab Chip 2024. https://doi.org/10.1039/d3lc00622k.

[36] Halldorsson S, Lucumi E, Gómez-Sjöberg R, Fleming RMT. Advantages and challenges of microfluidic cell culture in polydimethylsiloxane devices. Biosensors and Bioelectronics 2015;63:218–31. https://doi.org/10.1016/j.bios.2014.07.029.

[37] Lezzar DL, Lam FW, Huerta R, Mukhamedshin A, Lu M, Shevkoplyas SS. A high-throughput microfluidic device based on controlled incremental filtration to enable centrifugation-free, low extracorporeal volume leukapheresis. Sci Rep 2022;12:13798. https://doi.org/10.1038/s41598-022-16748-5.

[38] Barker C. Modernizing cell therapy manufacturing to reduce vein-to-vein times. BioInsights n.d. https://insights.bio/cell-and-gene-therapy-insights/journal/article/2907/Modernizing-cell-therapy-manufacturing-to-reduce-vein-to-vein-times (accessed September 5, 2023).

[39] Campos-González R, Skelley AM, Gandhi K, Inglis DW, Sturm JC, Civin CI, et al. Deterministic Lateral Displacement: The Next-Generation CAR T-Cell Processing? SLAS Technol 2018;23:338–51. https://doi.org/10.1177/2472630317751214.

[40] Civin CI, Ward T, Skelley AM, Gandhi K, Peilun Lee Z, Dosier CR, et al. Automated leukocyte processing by microfluidic deterministic lateral displacement. Cytometry Part A 2016;89:1073–83. https://doi.org/10.1002/cyto.a.23019.

[41] Philippidis A. Draper Aims High as a Kite against Cancer. GEN - Genetic Engineering and Biotechnology News 2020. https://www.genengnews.com/gen-edge/draper-aims-high-as-a-kite-against-cancer/ (accessed September 5, 2023).

[42] Vijayakumar V, Dabbi JM, Walker JL, Mertiri A, Christianson RJ, Fiering J. Rosette-induced separation of T cells by acoustophoresis. Biomicrofluidics 2022;16:054107. https://doi.org/10.1063/5.0109017.

[43] McCall D, Singh A, Biotechnology S. Enabling GMP-ready cell sorting n.d.

[44] Sugier HR, Bellebon L, Aider J-L, Larghero J, Peltzer J, Martinaud C. Feasibility of an acoustophoresis-based system for a high-throughput cell washing: application to bioproduction. Cytotherapy 2023;25:891–9. https://doi.org/10.1016/j.jcyt.2023.05.003.

[45] Cellular Highways: advancing cell sorting technology. TTP n.d. https://www.ttp.com/case-studies/cellular-highways-advancing-cell-sorting-technology/ (accessed September 14, 2023).

[46] Warkiani ME, Khoo BL, Tan DS-W, Bhagat AAS, Lim W-T, Yap YS, et al. An ultra-high-throughput spiral microfluidic biochip for the enrichment of circulating tumor cells. Analyst 2014;139:3245–55. https://doi.org/10.1039/c4an00355a.

[47] Kwon T, Yao R, Hamel J-FP, Han J. Continuous removal of small nonviable suspended mammalian cells and debris from bioreactors using inertial microfluidics. Lab Chip 2018;18:2826–37. https://doi.org/10.1039/C8LC00250A.

[48] Nivedita N, Papautsky I. Continuous separation of blood cells in spiral microfluidic devices. Biomicrofluidics 2013;7. https://doi.org/10.1063/1.4819275.

[49] Winter M, Hardy T, Rezaei M, Nguyen V, Zander-Fox D, Warkiani ME, et al. Isolation of Circulating Fetal Trophoblasts Using Inertial Microfluidics for Noninvasive Prenatal Testing. Advanced Materials Technologies 2018;3:1800066. https://doi.org/10.1002/admt.201800066.

[50] Zhang J, Yuan D, Sluyter R, Yan S, Zhao Q, Xia H, et al. High-Throughput Separation of White Blood Cells From Whole Blood Using Inertial Microfluidics. IEEE Transactions on Biomedical Circuits and Systems 2017.

[51] Warkiani ME, Tay AKP, Guan G, Han J. Membrane-less microfiltration using inertial microfluidics. Sci Rep 2015;5:11018. https://doi.org/10.1038/srep11018.

[52] Bhagat AAS, Kuntaegowdanahalli SS, Papautsky I. Continuous particle separation in spiral microchannels using dean flows and differential migration. Lab Chip 2008;8:1906–14. https://doi.org/10.1039/B807107A.

[53] Bhagat AAS, Kuntaegowdanahalli SS, Papautsky I. Continuous particle separation in spiral microchannels using dean flows and differential migration. Lab Chip 2008;8:1906–14. https://doi.org/10.1039/B807107A.

[54] Di Carlo D, Irimia D, Tompkins RG, Toner M. Continuous inertial focusing, ordering, and separation of particles in microchannels. Proceedings of the National Academy of Sciences 2007;104:18892–7. https://doi.org/10.1073/pnas.0704958104.

[55] Nivedita N, Papautsky I. Continuous separation of blood cells in spiral microfluidic devices. Biomicrofluidics 2013;7:54101. https://doi.org/10.1063/1.4819275.

[56] Lee K, Conboy M, Park HM, Jiang F, Kim HJ, Dewitt MA, et al. Nanoparticle delivery of Cas9 ribonucleoprotein and donor DNA in vivo induces homology-directed DNA repair.

Nature Biomedical Engineering 2017;1:889–901. https://doi.org/10.1038/s41551-017-0137-2.

[57] Arruga F, Gyau BB, Iannello A, Vitale N, Vaisitti T, Deaglio S. Immune Response Dysfunction in Chronic Lymphocytic Leukemia: Dissecting Molecular Mechanisms and Microenvironmental Conditions. Int J Mol Sci 2020;21. https://doi.org/10.3390/ijms21051825.

[58] Navas A, Giraldo-Parra L, Prieto MD, Cabrera J, Gómez MA. Phenotypic and functional stability of leukocytes from human peripheral blood samples: considerations for the design of immunological studies. BMC Immunology 2019;20:5. https://doi.org/10.1186/s12865-019-0286-z.

[59] Haselager MV, Kater AP, Eldering E. Proliferative Signals in Chronic Lymphocytic Leukemia; What Are We Missing? Front Oncol 2020;10. https://doi.org/10.3389/fonc.2020.592205.

[60] Kipps TJ, Stevenson FK, Wu CJ, Croce CM, Packham G, Wierda WG, et al. Chronic lymphocytic leukaemia. Nat Rev Dis Primers 2017;3:16096. https://doi.org/10.1038/nrdp.2016.96.

[61] Damle RN, Calissano C, Chiorazzi N. Chronic lymphocytic leukemia: a disease of activated monoclonal B cells. Best Pract Res Clin Haematol 2010;23:33–45. https://doi.org/10.1016/j.beha.2010.02.001.

[62] Riches JC, Davies JK, McClanahan F, Fatah R, Iqbal S, Agrawal S, et al. T cells from CLL patients exhibit features of T-cell exhaustion but retain capacity for cytokine production. Blood 2013;121:1612–21. https://doi.org/10.1182/blood-2012-09-457531.

[63] Bain BJ. Acute Lymphoblastic Leukaemia and Acute Leukaemia of Ambiguous Lineage. Leukaemia Diagnosis, John Wiley & Sons, Ltd; 2017, p. 249–94. https://doi.org/10.1002/9781119210511.ch4.

[64] Amin MM, Kermani S, Talebi A, Oghli MG. Recognition of Acute Lymphoblastic Leukemia Cells in Microscopic Images Using K-Means Clustering and Support Vector Machine Classifier. J Med Signals Sens 2015;5:49–58.

[65] Lacombe F, Durrieu F, Briais A, Dumain P, Belloc F, Bascans E, et al. Flow cytometry CD45 gating for immunophenotyping of acute myeloid leukemia. Leukemia 1997;11:1878–86. https://doi.org/10.1038/sj.leu.2400847.

[66] Gupta T, Gupta R, Mittal N, Rahman K, Nityanand S. B-acute Lymphoblastic Leukemia with Bright CD45 and Moderate Side Scatter Simulating Monocytoid Population: An Unusual Phenotype. Indian J Hematol Blood Transfus 2018;34:358–9. https://doi.org/10.1007/s12288-017-0896-7.

[67] Terwilliger T, Abdul-Hay M. Acute lymphoblastic leukemia: a comprehensive review and 2017 update. Blood Cancer J 2017;7:e577. https://doi.org/10.1038/bcj.2017.53.

[68] Vilchis-Ordoñez A, Contreras-Quiroz A, Vadillo E, Dorantes-Acosta E, Reyes-López A, Quintela-Nuñez del Prado HM, et al. Bone Marrow Cells in Acute Lymphoblastic Leukemia Create a Proinflammatory Microenvironment Influencing Normal Hematopoietic

Differentiation Fates. BioMed Research International 2015. https://doi.org/10.1155/2015/386165.

[69] Bienertova-Vasku J, Bienert P, Kodytkova D, Zlamal F, Tomandl J, Tomandlova M, et al. BAFF Levels Are Elevated in Paediatric Patients With Acute Lymphoblastic Leukaemia Compared to Other B-Lineage Neoplasms. Journal of Hematology 2012;1:20–2. https://doi.org/10.4021/.

[70] Chien CD, Hicks ED, Su PP, Qin H, Fry TJ. Precursor B Cell Acute Lymphoblastic Leukemia Induces Pro-Leukemic Changes in the Bone Marrow Microenvironment That Contribute to Therapeutic Resistance. Blood 2012;120:1466–1466. https://doi.org/10.1182/blood.V120.21.1466.1466.

[71] Amin HM, Yang Y, Shen Y, Estey EH, Giles FJ, Pierce SA, et al. Having a higher blast percentage in circulation than bone marrow: clinical implications in myelodysplastic syndrome and acute lymphoid and myeloid leukemias. Leukemia 2005;19:1567–72. https://doi.org/10.1038/sj.leu.2403876.

[72] DiNardo CD, Garcia-Manero G, Pierce S, Nazha A, Bueso-Ramos C, Jabbour E, et al. Interactions and relevance of blast percentage and treatment strategy among younger and older patients with acute myeloid leukemia (AML) and myelodysplastic syndrome (MDS). Am J Hematol 2016;91:227–32. https://doi.org/10.1002/ajh.24252.

[73] Ceppi F, Rivers J, Annesley C, Pinto N, Park JR, Lindgren C, et al. Lymphocyte apheresis for chimeric antigen receptor T-cell manufacturing in children and young adults with leukemia and neuroblastoma. Transfusion 2018;58:1414–20. https://doi.org/10.1111/trf.14569.

[74] Davis MM, Fesnak A, Leskowitz RM, McKee JS, Ohayon Y, Corl CM, et al. Predictors of manufacturing (MFG) success for chimeric antigen receptor (CAR) T cells in Non-Hodgkin Lymphoma (NHL). Cytotherapy 2017;19:S118–9. https://doi.org/10.1016/j.jcyt.2017.02.190.

[75] Fesnak AD, Hanley PJ, Levine BL. Considerations in T Cell Therapy Product Development for B Cell Leukemia and Lymphoma Immunotherapy. Curr Hematol Malig Rep 2017;12:335–43. https://doi.org/10.1007/s11899-017-0395-9.

[76] Figueiredo M. CAR T-cell Therapy Tecartus for Mantle Cell Lymphoma Gets FDA Nod 2020. https://immuno-oncologynews.com/2020/07/28/car-t-cell-therapy-tecartus-granted-fda-approval-for-mantle-cell-lymphoma/ (accessed September 14, 2020).

[77] Stanton D. Kite flies high with second CAR-T approval - Bioprocess Insider. BioProcess International 2020. https://bioprocessintl.com/bioprocess-insider/regulations/kite-flies-high-with-second-car-t-approval/ (accessed September 3, 2020).

[78] Qayed M, McGuirk JP, Myers GD, Parameswaran V, Waller EK, Holman P, et al. Leukapheresis guidance and best practices for optimal chimeric antigen receptor T-cell manufacturing. Cytotherapy 2022;24:869–78. https://doi.org/10.1016/j.jcyt.2022.05.003.

[79] Xu Y, Zhang M, Ramos CA, Durett A, Liu E, Dakhova O, et al. Closely related T-memory stem cells correlate with in vivo expansion of CAR.CD19-T cells and are preserved by IL-7 and IL-15. Blood 2014;123:3750–9. https://doi.org/10.1182/blood-2014-01-552174.

[80] Aksoy P, Aksoy BA, Czech E, Hammerbacher J. Electroporation characteristics of human primary T cells. bioRxiv 2019:466243. https://doi.org/10.1101/466243.

[81] Idris S-Z, Hassan N, Lee L-J, Md Noor S, Osman R, Abdul-Jalil M, et al. Increased regulatory T cells in acute lymphoblastic leukaemia patients. Hematology 2016;21:206–12. https://doi.org/10.1080/10245332.2015.1101965.

[82] Sudarsanam H, Buhmann R, Henschler R. Influence of Culture Conditions on Ex Vivo Expansion of T Lymphocytes and Their Function for Therapy: Current Insights and Open Questions. Front Bioeng Biotechnol 2022;10:886637. https://doi.org/10.3389/fbioe.2022.886637.

[83] Jenkins Y, Zabkiewicz J, Ottmann O, Jones N. Tinkering under the Hood: Metabolic Optimisation of CAR-T Cell Therapy. Antibodies (Basel) 2021;10:17. https://doi.org/10.3390/antib10020017.

[84] Niedźwiecki M, Budziło O, Adamkiewicz-Drożyńska E, Pawlik-Gwozdecka D, Zieliński M, Maciejka-Kembłowska L, et al. CD4+CD25highCD127low/-FoxP3+ Regulatory T-Cell Population in Acute Leukemias: A Review of the Literature. J Immunol Res 2019;2019:2816498. https://doi.org/10.1155/2019/2816498.

[85] Paluskievicz CM, Cao X, Abdi R, Zheng P, Liu Y, Bromberg JS. T Regulatory Cells and Priming the Suppressive Tumor Microenvironment. Front Immunol 2019;10. https://doi.org/10.3389/fimmu.2019.02453.

[86] Wolf AM, Wolf D, Steurer M, Gastl G, Gunsilius E, Grubeck-Loebenstein B. Increase of Regulatory T Cells in the Peripheral Blood of Cancer Patients. Clin Cancer Res 2003;9:606–12.

[87] Goudin N, Chappert P, Mégret J, Gross D-A, Rocha B, Azogui O. Depletion of Regulatory T Cells Induces High Numbers of Dendritic Cells and Unmasks a Subset of Anti-Tumour CD8+CD11c+ PD-1lo Effector T Cells. PLOS ONE 2016;11:e0157822. https://doi.org/10.1371/journal.pone.0157822.

[88] Morse MA, Hobeika AC, Osada T, Serra D, Niedzwiecki D, Lyerly HK, et al. Depletion of human regulatory T cells specifically enhances antigen-specific immune responses to cancer vaccines. Blood 2008;112:610–8. https://doi.org/10.1182/blood-2008-01-135319.

[89] Attia P, Powell DJ, Maker AV, Kreitman RJ, Pastan I, Rosenberg SA. Selective Elimination of Human Regulatory T Lymphocytes In Vitro With the Recombinant Immunotoxin LMB-2. J Immunother 2006;29:208–14. https://doi.org/10.1097/01.cji.0000187959.45803.0c.

[90] Malek TR. The main function of IL-2 is to promote the development of T regulatory cells. J Leukoc Biol 2003;74:961–5. https://doi.org/10.1189/jlb.0603272.

[91] Lissandrello C, Dubay R, Kotz KT, Fiering J. Purification of Lymphocytes by Acoustic Separation in Plastic Microchannels. SLAS Technol 2018;23:352–63. https://doi.org/10.1177/2472630317749944.

[92] Chiaretti S, Zini G, Bassan R. Diagnosis and Subclassification of Acute Lymphoblastic Leukemia. Mediterr J Hematol Infect Dis 2014;6. https://doi.org/10.4084/MJHID.2014.073.

[93] King JF, Lam JT. A Practical Approach to Diagnosis of B-Cell Lymphomas With Diffuse Large Cell Morphology. Archives of Pathology & Laboratory Medicine 2020;144:160–7. https://doi.org/10.5858/arpa.2019-0182-RA.

[94] Elsemary MT, Maritz MF, Smith LE, Warkiani M, Bandara V, Napoli S, et al. Inertial Microfluidic Purification of CAR-T-Cell Products. Advanced Biology 2022;6:2101018. https://doi.org/10.1002/adbi.202101018.

[95] Tian Y, Hu R, Du G, Xu N. Microfluidic Chips: Emerging Technologies for Adoptive Cell Immunotherapy. Micromachines 2023;14. https://doi.org/10.3390/mi14040877.

[96] Producing CAR T cell therapy at a lower cost. News-Medical 2020. https://www.news-medical.net/news/20200623/Producing-CAR-T-cell-therapy-at-a-lower-cost.aspx (accessed April 21, 2024).

[97] Ran T, Eichmüller SB, Schmidt P, Schlander M. Cost of decentralized CAR T-cell production in an academic nonprofit setting. Int J Cancer 2020;147:3438–45. https://doi.org/10.1002/ijc.33156.

[98] Decentralized CAR-T Manufacturing Reduces Costs & Complexity, Expands Access n.d. https://www.cellandgene.com/doc/decentralized-car-t-manufacturing-reduces-costs-complexity-expands-access-0001 (accessed April 21, 2024).

[99] Do TD, Pham UT, Nguyen LP, Nguyen TM, Bui CN, Oliver S, et al. Fabrication of a Low-Cost Microfluidic Device for High-Throughput Drug Testing on Static and Dynamic Cancer Spheroid Culture Models. Diagnostics 2023;13:1394. https://doi.org/10.3390/diagnostics13081394.

[100] Rodríguez CF, Andrade-Pérez V, Vargas MC, Mantilla-Orozco A, Osma JF, Reyes LH, et al. Breaking the clean room barrier: exploring low-cost alternatives for microfluidic devices. Front Bioeng Biotechnol 2023;11:1176557. https://doi.org/10.3389/fbioe.2023.1176557.

[101] Even-Or E, Di Mola M, Ali M, Courtney S, McDougall E, Alexander S, et al. Optimizing autologous nonmobilized mononuclear cell collections for cellular therapy in pediatric patients with high-risk leukemia. Transfusion 2017;57:1536–42. https://doi.org/10.1111/trf.14094.

[102] Warkiani ME, Khoo BL, Tan DS-W, Bhagat AAS, Lim W-T, Yap YS, et al. An ultra-high-throughput spiral microfluidic biochip for the enrichment of circulating tumor cells. Analyst 2014;139:3245–55. https://doi.org/10.1039/C4AN00355A.

[103] Dubay R, Lissandrello C, Swierk P, Moore N, Doty D, Fiering J. Scalable high-throughput acoustophoresis in arrayed plastic microchannels. Biomicrofluidics 2019;13:034105. https://doi.org/10.1063/1.5096190.